IEEE Access
Multidisciplinary | Rapid Review | Open Access Journal

Received 14 November 2024, accepted 26 November 2024, date of publication 18 December 2024,
date of current version 30 December 2024.

Digital Object Identifier 10.1109/ACCESS.2024.3520104

RESEARCH ARTICLE

Multitone QAM Modulation Design for Simultaneous Wireless Information and Power Transfer

PRERNA DHULL[1,2], (Graduate Student Member, IEEE), NEGIN SHARIATI[2], (Senior Member, IEEE), SOFIE POLLIN[1], (Senior Member, IEEE), MEHRAN ABOLHASAN[2], (Senior Member, IEEE), AND DOMINIQUE SCHREURS[1], (Fellow, IEEE)

[1]Division WaveCoRE, Department of Electrical Engineering (ESAT), KU Leuven, Leuven 3001, Belgium
[2]RF and Communication Technologies (RFCT) Research Laboratory, University of Technology Sydney, Sydney, NSW 2007, Australia

Corresponding author: Prerna Dhull (prerna.dhull@student.uts.edu.au)

This work is supported in part by the SUPERIOT-Truly Sustainable Printed Electronics-based IoT combining Optical and Radio Wireless Technologies Project through the Smart Networks and Services Joint Undertaking (SNS JU) under European Union's Horizon Europe Research and Innovation Programme under Grant 101096021; in part by the Flemish Fonds voor Wetenschappelijk Onderzoek—Vlaanderen (FWO) Strategisch Basisonderzoek (SBO) Sustainable Internet of Battery-Less Things (IoBaLeT) Project S001521N; and in part by the Massive Backscattering for High Throughput Zero Power Wireless Networking Project FWO G085818N.

ABSTRACT Future Internet of Things (IoT) networks are expected to realize far-field wireless power transfer (WPT) to mitigate the sensors' dependence on batteries. Recently, simultaneous wireless information and power transfer (SWIPT) has gained attention by utilizing RF signals for both information as well as power transfer. In this paper, a novel N-tone multitone quadrature-amplitude-modulation (QAM) transmission waveform carrying $(N-1)$ information symbols, is proposed for an integrated information-energy receiver with a lower power consumption compared to conventional separated information-energy receiver architectures. The multitone QAM signal is designed by exploiting the non-linearity of the receiver-rectifier, and both amplitudes and phases are used for information transfer offering an advantage of a higher degree of freedom to optimize WPT and wireless information transfer (WIT) performances. It is shown that the power performance of the designed waveform varies with the orientation of the symbol constellation. Two asymmetric QAM constellation designs, expanded symbol constellation and compressed symbol constellation, are proposed to enhance WPT performance according to the application-specific requirement, such as whether a higher level of minimum continuous power transfer is critical or if a high-power transfer in short bursts is preferred for the SWIPT's operation. It has been shown that WPT and WIT performances can be enhanced according to the IoT node's requirements by varying the transmission probabilities of inner symbols and outer symbols of the QAM constellation.

INDEX TERMS Energy harvesting, Internet of Things, modulation technique, quadrature amplitude modulation (QAM), signal design, simultaneous wireless information and power transfer (SWIPT), waveform design, wireless power transfer (WPT).

I. INTRODUCTION

The applications of Internet of Things (IoT) with enhanced sensing capabilities have been expanding to a diverse range of domains such as agriculture, smart cities, transportation, wearable devices, and homes [1]. The rapid surge of IoT devices has raised the challenge of periodically charging/replacing batteries. Far-field radio-frequency (RF) wireless power transfer (WPT) offers a promising solution for reducing the reliance of sensors on batteries [2].

The associate editor coordinating the review of this manuscript and approving it for publication was Alon Kuperman.

Simultaneous wireless information and power transfer (SWIPT) integrates far-field WPT with wireless information transfer (WIT) and provides an energy-efficient solution by exploiting the same communication signal for power transfer earlier used for data transfer solely [3], [4].

A vast amount of research on SWIPT has been performed for a separated information-energy receiver architecture where power transfer and information decoding are performed independently by separate modules [5]. For this, the received signal is split into two paths using power splitting, time-switching, antenna switching, or frequency splitting [6], [7], [8], [9], [10]. However, this independent WIT and WPT processing provides a lower system integration between WIT and WPT. Therefore, researchers introduced another category of integrated information-energy receiver architecture where diodes for rectification are used for power transfer as well as for RF to baseband conversion for information decoding [5]. This architecture offers the benefit of reducing circuit complexity and power consumption at the SWIPT receiver by removing the power-consuming mixing operation for information decoding, making it more suitable for simple IoT devices [3].

In the integrated SWIPT architecture, conventional communication signals are not possible to be used for information decoding after rectification through diodes. Therefore, new communication signals need to be proposed for an integrated reception of power and information at the rectifier output. Research has been conducted to improve the rectifier's power conversion efficiency (PCE) [11], [12]. It has been shown that due to the non-linearity introduced by the rectifier, the rectifier output DC power is not only a function of received signal power and rectenna design but also is a function of the received signal's shape [13], [14], [15]. High peak-to-average-power ratio (PAPR) waveforms have been shown to exploit this non-linearity to improve the harvested DC power [16], [17].

A single-tone modulation signal for integrated architecture is introduced in [5], where information symbols are transmitted with different energy levels through a rectifier. Pulse-position modulation for integrated receivers has been introduced in [15]. In [18] and [19], the authors present methods which utilize multitone signals for higher PAPR. Information symbols are transmitted by varying the number of tones and frequency spacing between tones based on the transmitted information, which results in varying signal PAPR. A two-dimensional signaling scheme with subcarrier number component and amplitude component is introduced in [20], where information is transmitted in signal PAPR variation due to varying numbers of subcarriers and amplitudes of subcarriers.

An amplitude-based biased-ASK is introduced where a minimum non-zero amplitude is transmitted to avoid periods of zero energy harvesting [21]. A dual ASK scheme for a double half-wave rectifier is proposed, having a higher degree of freedom for signal amplitudes' constellation range, increasing the information rate [22]. Recently, a customized

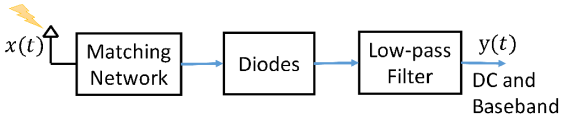

FIGURE 1. Integrated information-energy receiver rectifier for SWIPT.

on-off keying scheme for Terahertz imaging with simultaneous information and power transfer with the help of an integrated receiver has been proposed in [23]. However, a single-tone communication signal does not benefit the high PAPR signals for improved energy harvesting. A modulation technique that uses a multitone signal is introduced in [24] where a model of embedding information in the ratios of the amplitudes of the different tones is proposed rather than in the amplitudes directly. Although it offers the advantage of making the system less dependent on transmission distance, the drawback of this technique is that it is not suitable for more than a three-tone signal.

Amplitude variations impose a limit on achievable WPT due to the presence of ripples in the output voltage that degrade the WPT performance [21], [24]. Multitone FSK has been introduced in [25] and [26] where information symbols are transmitted through rectifier by varying frequency spacings among tones, and a Fast Fourier transform (FFT) is used for information decoding. A Multitone PSK modulation technique is introduced in [27] where tones's phases are used for transmitting multiple symbols over a single multitone transmission. It is shown that for Multitone PSK, the output PCE does not vary much with information transmission as was the case with amplitude-based schemes.

Although Multitone PSK offers the advantage of minimizing the effect of information transfer over the SWIPT system's power performance compared to amplitude-based schemes, amplitude-based schemes are beneficial in the case of a noisy channel [28], [29], [30]. Till now, either the multitone signal amplitudes or only the multitone signal phases have been exploited for information transfer through integrated receiver architecture. An ideal waveform for a SWIPT system would entail minimal variations in the envelope, with the stream of information symbols having an approximately stable WPT while also having a good data transfer rate. Therefore, a higher data rate can be achieved by the simultaneous usage of both amplitudes and phases of the multitone signal for information transfer.

This paper presents the design of a novel multitone quadrature amplitude modulation (QAM) transmission scheme utilizing multitone signal's amplitudes, phases, and number of tones for the integrated information-energy SWIPT receiver architecture. Both amplitudes and phases of tones are utilized for information transmission for a higher data rate. Power transfer and data reception are performed from the same rectified output signal. The impact of QAM symbol constellation on the PAPR of the designed multitone waveform is studied. Further, a redesign of QAM

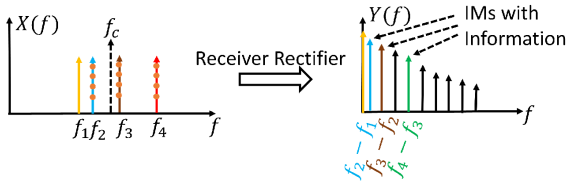

FIGURE 2. Four-tone multitone QAM RF signal frequency spectrum $X(f)$ centered around frequency $f_c = 2.45$ GHz and rectified baseband output spectrum $Y(f)$ consisting of dc, IM frequency tones used for information decoding (colored), and extra IM components (black).

symbol constellations for a more stable output PCE is proposed to minimize the difference between the achievable PCE of the rectifier for different transferred symbols. In particular, asymmetric expanded QAM constellation and asymmetric compressed QAM constellation are proposed to allow trade-offs of application-specific demands such as power demands, symbol error rate, and data rate. Further, probabilities of transmission probabilities of inner symbols and outer symbols can be varied to enhance the performance.

Multitone QAM offers the advantage of a higher degree of freedom to optimize PCE, information rate, and symbol error rate by utilizing amplitudes, phases, and number of tones. It is possible to transmit $(N-1)$ symbols over a single stream of an N-tone Multitone QAM signal resulting in an OFDM-type communication with non-uniform frequency spacings for the integrated information-energy receiver where RF to baseband conversion is performed with a simple rectifier circuitry, removing the need for a local oscillator at the receiver. It is shown that due to the non-linearity of the rectifier, it is important to redesign the QAM constellation according to the application-specific requirements, such as such as whether a higher level of minimum continuous power transfer is critical or if a high-power transfer in short bursts is preferred for the SWIPT's operation.

This paper is organized as follows. Section II introduces the theoretical design of a multitone QAM signal and analyses the effect of symbol constellation over the resulting PAPR of the designed waveform. Next, section III-A discusses the proposed redesigned asymmetric QAM constellations. Then, the performance of the proposed multitone QAM signal and proposed asymmetric QAM constellation designs are analysed in Section IV. In the end, a conclusion is drawn in Section V.

II. SIGNAL MODEL

The integrated rectifier-receiver illustrated in Fig. 1 consisting of an input matching network, rectifier diodes, and a resistance-capacitance (RC)-low-pass filter (LPF) is utilized for both WPT and WIT simultaneously. Multitone QAM signal $x(t)$ is designed using an N-tone multitone signal and modifying the tones' amplitudes and phases according to the transmitted QAM information symbols. $x(t)$ is designed around the center frequency f_c of 2.45 GHz. The received signal $x(t)$ is passed through the rectifier, and subsequently, the baseband rectified signal output $y(t)$ is used for both power transfer and information decoding.

A. SIGNAL DESIGN

An N-tone reference signal $r(t)$ with an average power of P_{in} is considered as

$$r(t) = \text{Re}\left\{\sum_{n=1}^{N}\sqrt{\frac{2P_{\text{in}}}{N}}e^{j(2\pi f_n t)}\right\}. \tag{1}$$

$(N-1)$ information symbols are transmitted over an N-tone multitone QAM signal. The N-tones multitone signal with non-uniform frequency spacings is used to utilize the non-linearity of the rectifier. QAM information is transmitted in amplitudes and phases of the tones of the multitone signal $r(t)$. The transmitted multitone QAM signal $x(t)$ after modifying the tones' amplitudes and phases of $r(t)$ in (1) according to the transmitted information, can be represented as

$$x(t) = \text{Re}\left\{\sum_{n=1}^{N}\sqrt{\frac{2|s_{n-1}|P_{\text{in}}}{N|s|_{\max}}}e^{j(2\pi f_n t+\phi_n)}\right\} \tag{2}$$

where each n^{th} tone of $r(t)$ has been modified to include the transmitted information symbol s_{n-1}. $|s|_{\max}$ represents the maximum available magnitude among M information symbols, i.e., $|s_{\sqrt{M},\sqrt{M}}|$. The first tone is considered constant, with s_0 being 1. In this way, $(N-1)$ symbols are transmitted over a single multitone transmission. Information symbols s_n are selected from the available information set $\boldsymbol{S}$ of M QAM symbols for the modulation order of M. The M information symbols can be represented as

$$s_{i,k} = |s_{i,k}|e^{j\phi_{i,k}}, \quad \forall \ \ i,k = \{1,2,\cdots,\sqrt{M}\}. \tag{3}$$

Information is transmitted through the amplitudes and phases of the tones of the multitone QAM signal as represented in (2). $(N-1)$ information symbols are transmitted with a single stream of N-tone multitone QAM signal. For each n^{th} tone, s_{n-1} and ϕ_n of (2) are modified according to the chosen transmitted information symbol $s_{i,k}$ from set $\boldsymbol{S}$ of (3).

The spectra of the multitone QAM signal $X(f)$ and the rectified baseband output signal $Y(f)$ are shown in Fig. 2. The essence is a block of N tones with non-uniform frequency spacing so that the intermodulation frequencies of the different tones can be found at different frequencies. N-tones multitone QAM signal is designed to carry $(N-1)$ information symbols. The information is transmitted through both the tones' amplitudes and phases. The non-linearity of the rectifier is utilized to extract the transmitted information from the baseband signal $y(t)$ at the rectifier output. Due to the non-linearity of the rectifier, an N-tone multitone signal, after passing through the rectifier, produces a baseband signal that includes intermodulation (IM) frequency components of various orders, resulting from the mixing of the different tones in the multitone QAM signal [31]. These IM frequency components result in ripple voltage at the rectifier output in addition to the required output DC.

Although the presence of ripple voltage is not efficient for wireless power transfer, these ripples can be used for wireless information transfer and decoding through the same rectifier-receiver, lowering the power consumption for signal processing at the receiver. Therefore, the rectifier's non-linearity is exploited to bring the information down to the baseband at the receiver. The signal is designed so that the information resides in the intermodulation products present at baseband frequencies in the output of the integrated rectifier-receiver.

Among IM frequency components of various orders produced at the rectifier output due to mixing among the tones of the multitone QAM signal, the second-order intermodulation (IM_2) frequency components dominate at the receiver output compared to higher-order IM components [32]. The second-order IM frequency components are the result of mixing between two tones of a multitone QAM signal. In our work, we encode information in a multitone QAM signal in such a way that information at the rectifier output would be extracted from the IM_2 frequency components between consecutive frequency tones. For this, multitone QAM signal tones' frequencies are designed in such a way that these desired IM_2 do not overlap with each other. Hence, Algorithm 1 of [27] is used to design such an unequal-spaced multitone signal.

The rectified baseband output $y(t)$ consists of dc and several intermodulation frequency components due to the rectifier's non-linearity. However, all the odd order 3^{rd} order, 5^{th} order, $\cdots$, etc., intermodulation frequency components lie in the GHz frequency range, and all the even order 4^{th} order, 6^{th} order, $\cdots$, etc., intermodulation frequency components lie in the baseband frequency range. All the odd-order intermodulation frequency components are filtered out by the LPF, and $y(t)$ consists of only dc and even-order intermodulation frequency components. Therefore, as a result of LPF after diodes at the output, $y(t)$ results in a baseband signal consisting of only dc and intermodulation frequency components in the MHz frequency range. Furthermore, second-order IM frequency components dominate among these even-order intermodulation frequency components [32].

For example, from (2), $x(t)$ for a three-tone signal can be represented by

$$\begin{aligned} x(t) = &\sqrt{\frac{2|s_0|P_{\text{in}}}{N|s|_{\max}}}\cos(2\pi f_1 t + \phi_0) \\ &+ \sqrt{\frac{2|s_1|P_{\text{in}}}{N|s|_{\max}}}\cos(2\pi f_2 t + \phi_1) \\ &+ \sqrt{\frac{2|s_2|P_{\text{in}}}{N|s|_{\max}}}\cos(2\pi f_3 t + \phi_2) \end{aligned} \tag{4}$$

The signal (4) after passing through the rectifier results in rectified baseband signal $y(t)$ consisting of dc and three second-order IM frequency components among tones as

$$\begin{aligned} y(t) \propto \text{dc} &+ \sqrt{|s_0||s_1|}\frac{2P_{\text{in}}}{N|s|_{\max}}\cos(2\pi(f_2 - f_1)t + \phi_1 - \phi_0) \\ &+ \sqrt{|s_1||s_2|}\frac{2P_{\text{in}}}{N|s|_{\max}}\cos(2\pi(f_3 - f_2)t + \phi_2 - \phi_1) \\ &+ \sqrt{|s_0||s_2|}\frac{2P_{\text{in}}}{N|s|_{\max}}\cos(2\pi(f_3 - f_1)t + \phi_2 - \phi_0) \end{aligned} \tag{5}$$

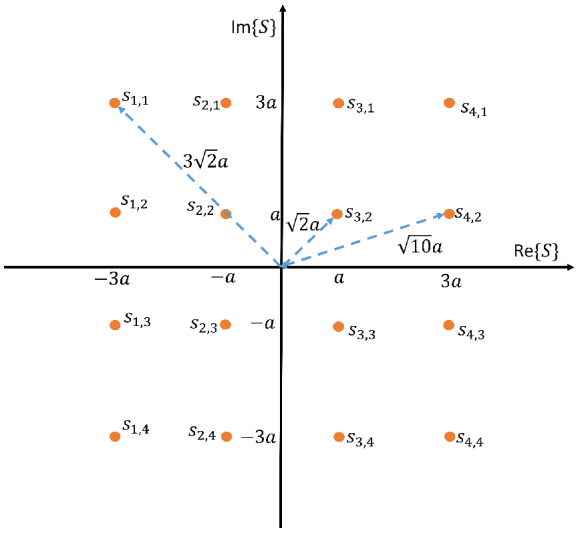

FIGURE 3. Symbol constellation for multitone QAM with modulation order of $M = 16$.

Here, $(N-1)$ information symbols are considered to be transmitted over an N-tone multitone signal. The first tone f_1 is assumed to be transmitted with a constant amplitude of $\sqrt{2P_{\text{in}}/N}$ and phase 0°, i.e., $|s_0| = 1$ and $\phi_0 = 0°$. The multitone signal is designed in such a way that $(N-1)$ intermodulation baseband tones as a result of consecutive frequency tones would consist of $(N-1)$ information symbols at the rectifier output, i.e., $(f_2 - f_1)$, $(f_3 - f_2)$, $\cdots$, $(f_N - f_{N-1})$ baseband tones amplitudes would carry the information as shown in Fig. 2. A 4-tone multitone signal is depicted in Fig. 2 with the first tone having constant amplitude and phase, and three information symbols from the available symbol set $\boldsymbol{S}$ are transmitted over the other three tones of $x(t)$. SWIPT is achieved at the output by both WIT and WPT from the same rectified signal. The whole output baseband signal is utilized for power transfer, whereas three information symbols are decoded by analysing the three relevant baseband tones $(f_2 - f_1)$, $(f_3 - f_2)$, and $(f_4 - f_3)$' magnitudes and phases as shown in Fig. 2.

To ensure that the $(N-1)$ desired baseband tones at the rectifier output are distinct, the N-tone multitone signal is designed so that the second-order intermodulation IM_2 frequency components between consecutive tones do not overlap. Specifically, the baseband tones $(f_2 - f_1)$, $(f_3 - f_2)$, $\cdots$ $(f_N - f_{N-1})$ should be distinct from one another and also these

$(N-1)$ baseband tones should not coincide with any other non-consecutive IM_2s. Therefore, to make SWIPT feasible with only a rectifier-receiver, the N-tone multitone signal does not consist of equally spaced tones around the central frequency of 2.45 GHz and needs to have unequal frequency spacings between tones. We proposed an algorithm to design this frequency spacing in [27]. Here, Algorithm 1 from [27] is used to define the tone frequencies of the multitone QAM signal.

QAM constellation for a modulation order of $M = 16$ is shown in Fig. 3. M-ary QAM can be considered as a combination of two $\sqrt{M}$-ary Pulse Amplitude Modulation (PAM) with a quadrature phase difference between them [33]. Let b_i denote the PAM constellation with $\sqrt{M}$ symbols represented as

$$b_i = -(\sqrt{M}-1) + (i-1)\frac{\sqrt{M}}{2}, \quad \forall \ i = \{1, 2, \cdots, \sqrt{M}\}. \tag{6}$$

Then, the QAM symbols can be represented as a combination of two PAM symbols constellations as

$$s_{i,k} = b_i + jb_k, \quad \forall \ i,k = \{1, 2, \cdots, \sqrt{M}\} \tag{7}$$

resulting in M symbols and depicted in Fig. 3. Further, QAM symbols are normalized with respect to the maximum available magnitude of symbols $|s_{\sqrt{M},\sqrt{M}}|$ and can be represented as

$$s_{i,k} = \frac{b_i + jb_k}{|s_{\sqrt{M},\sqrt{M}}|} = \frac{b_i + jb_k}{\sqrt{b_{\sqrt{M}} + jb_{\sqrt{M}}}}, \quad \forall \ i,k = \{1, 2, \cdots, \sqrt{M}\}. \tag{8}$$

After normalization, the maximum available magnitude among M information symbols $s_{\sqrt{M},\sqrt{M}}$ would be 1 in all symbol constellations. $(N-1)$ symbols in (2) are chosen from the available normalized information symbol set $(\boldsymbol{S})$ in (8) consisting of M symbols $s_{1,1}, s_{1,2}, \cdots, s_{\sqrt{M},\sqrt{M}}$.

B. PAPR ANALYSIS

In the proposed multitone QAM transmission scheme, the reference multitone signal $r(t)$ is modified to multitone QAM signal $x(t)$ by varying the tones' amplitudes and phases as in (2) to make the WIT possible in addition to WPT. The resulting average power of the transmitted SWIPT signal, P_{avg}, after embedding information becomes lower than P_{in}, i.e., $P_{\text{avg}} \leq P_{\text{in}}$. Therefore, it is important to analyze the effect of WIT with QAM symbols on the WPT performance of the SWIPT system. Here, PAPR is considered as a figure of merit for evaluating WPT performance as high PAPR waveforms result in higher harvested energy [13]. For electronics systems designed only for WPT, $r(t)$ would achieve maximum PAPR and the corresponding maximum PCE as no information is being transmitted. However, it is necessary to compromise a little with the WPT performance to design signals for SWIPT systems for additional usage of resources. The channel is considered ideal, i.e., there is no signal distortion between transmitter and receiver, and the performance of the designed signal $x(t)$ is analysed.

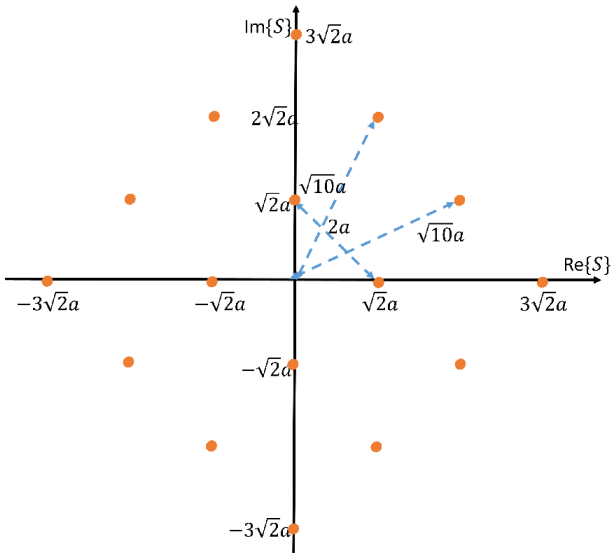

FIGURE 4. Rotated symbols constellations for QAM multitone for a modulation order of $M = 16$ with a phase shift of 45°.

PAPR for a signal $x(t)$ can be represented by

$$\text{PAPR} = \frac{P_{\text{peak}}}{P_{\text{avg}}} = \frac{max\{|x(t)|^2\}}{\frac{1}{T}\int_{-T/2}^{T/2} x^2(t)dt}, \tag{9}$$

where T denotes the time-period of waveform $x(t)$. The peak power of a multitone QAM signal in (2) can be represented as

$$P_{\text{peak}} = \frac{2P_{\text{in}}}{N} \times \left|1 + \sqrt{\frac{|s_1|}{|s_{\sqrt{M},\sqrt{M}}|}}\cos\phi_1 + \cdots + \sqrt{\frac{|s_{N-1}|}{|s_{\sqrt{M},\sqrt{M}}|}}\cos\phi_{N-1}\right|^2. \tag{10}$$

The average power of multitone QAM signal, P_{avg}, can be represented as

$$P_{\text{avg}} = \frac{P_{\text{in}}}{N}\left(1 + \frac{|s_1|}{|s_{\sqrt{M},\sqrt{M}}|} + \cdots + \frac{|s_{N-1}|}{|s_{\sqrt{M},\sqrt{M}}|}\right). \tag{11}$$

Therefore, from (9), (10), and (11), the PAPR for the multitone QAM signal $x(t)$ in terms of $(N-1)$ transmitted symbols can be represented as

$$\text{PAPR} = \frac{2\left|\sqrt{|s_{\sqrt{M},\sqrt{M}}|} + \sqrt{|s_1|}\cos\phi_1 + \cdots + \sqrt{|s_{N-1}|}\cos\phi_{N-1}\right|^2}{|s_{\sqrt{M},\sqrt{M}}| + |s_1| + |s_2| + \cdots + |s_{N-1}|}. \tag{12}$$

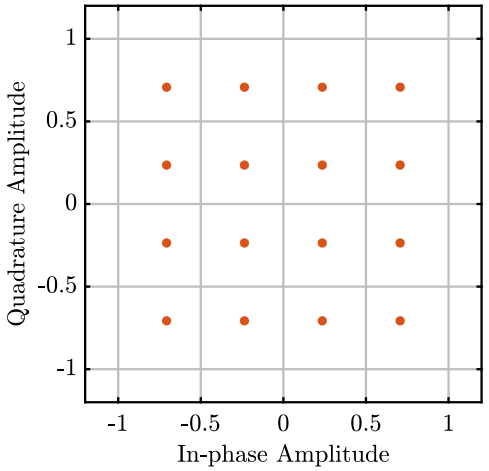

(a)

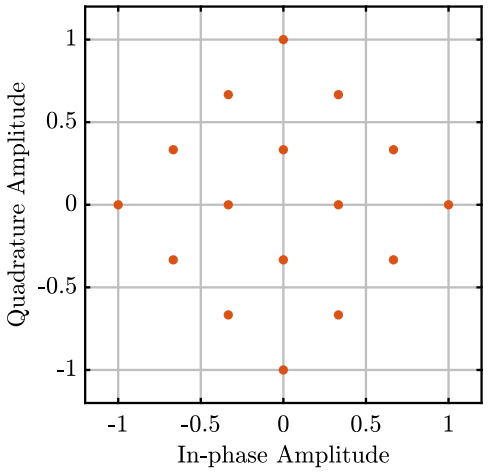

(b)

FIGURE 5. Normalized symbols constellations for $M = 16$ QAM (a) conventional and (b) with phase rotation of 45°.

The mean PAPR across the multitone signal streams with QAM streams can be represented as

$$\text{PAPR}|_{\text{mean}} = \frac{2\left|\sqrt{|s|_{\max}}\cos\phi_1 + \left(\frac{N-1}{M}\right)\sum_{i=1}^{M}\sqrt{|s_i|}\cos\phi_i\right|^2}{|s|_{\max} + \left(\frac{N-1}{M}\right)\sum_{i=1}^{M}|s_i|}. \quad (13)$$

It can be seen that the effect of symbol phases, in addition to symbol magnitudes, also plays a role in determining the signal PAPR. It is well known that multitone signals with tones' phases zero result in the highest PAPR [34]. Therefore, symbol constellations can be modified to maximize the multitone QAM signal PAPR. Fig. 4 illustrates a rotated symbol constellation for the 16-QAM symbol in Fig. 3 such that now, symbols with maximum magnitudes have zero phases. The average symbol energy remains the same as the rotation of symbols does not change the overall average symbols energy [33]. Fig. 5(a) and Fig. 5(b) illustrate the normalized 16-QAM constellation without and with phase rotation, respectively.

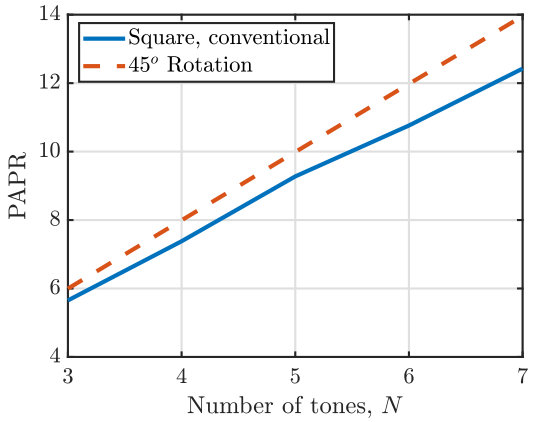

FIGURE 6. Multitone QAM signal PAPR with conventional QAM symbols constellation and the QAM symbols constellation rotated with 45°.

Variation in PAPR of transmitted waveform $x(t)$ with the number of tones N is illustrated in Fig. 6. It can be seen that with the phase shifting of the symbols' constellation, it is possible to achieve the maximum possible PAPR of $2N$ for the transmission of symbols carrying the highest energy. Therefore, by modifying only the phases of the symbols constellation, PAPR improves. However, the magnitudes of individual symbols remain the same. For further improvement in signal PAPR and in-turn output PCE, it is necessary to observe the effect of variations in symbols' magnitudes.

III. ASYMMETRIC QAM CONSTELLATION

In SWIPT communication, WPT performance is reduced because of the simultaneous WIT transfer. Due to information transfer over the same signal for SWIPT, the overall average power of the signal stream varies and the PCE at the output is lower compared to the achievable PCE for the case of a solely WPT. Therefore, it becomes important to look for ways to maximize the output of PCE while simultaneously transmitting information symbols.

Conventional QAM symbols constellation and the rotated QAM constellation discussed in the previous section, are symmetric in magnitude and do not consider the non-linearity of the rectifier. Such symmetric symbol constellations do not perform efficiently for power delivery at the rectifier output due to the non-linearity of the rectifier. Therefore, asymmetric QAM constellations need to be designed to achieve maximum PCE while simultaneously having good information detection at the rectifier output.

A. QAM CONSTELLATION REDESIGN

To design an asymmetric $\sqrt{M}$-PAM constellation $\boldsymbol{B}_{\text{asym},\sqrt{M}}$ from a symmetric $\sqrt{M}$-PAM constellation $\boldsymbol{B}_{\sqrt{M}}$, a multiplication factor $\boldsymbol{\Delta B}_{\sqrt{M}}$ is evaluated. Let $\boldsymbol{B}_{\sqrt{M}}$ be a square $\sqrt{M} \times \sqrt{M}$ matrix having the symmetric $\sqrt{M}$-PAM

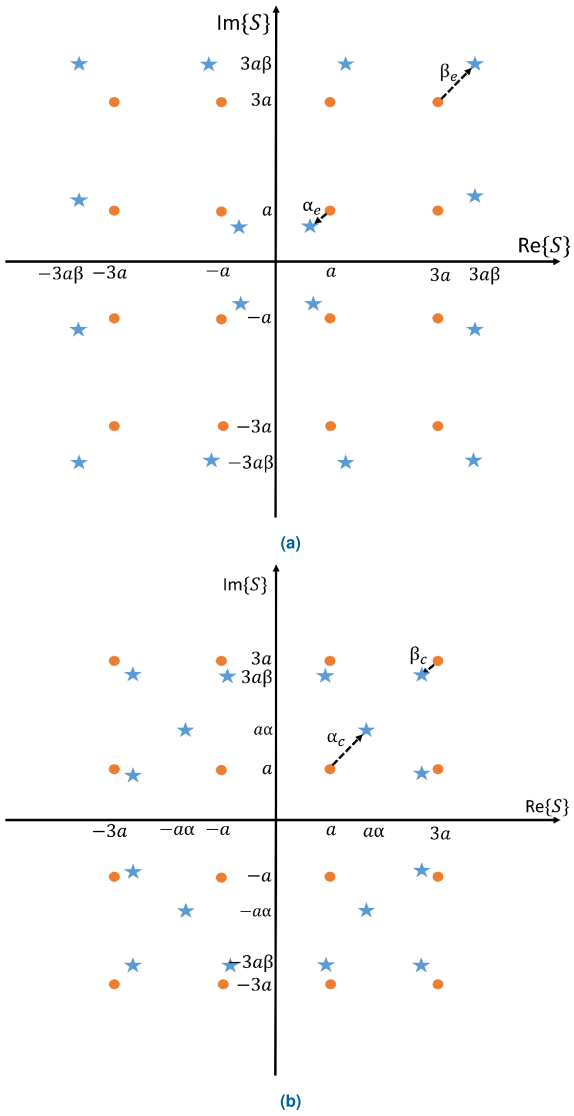

FIGURE 7. (a) Modified expanded Multitone QAM symbols constellations with $\alpha_e \leq 1$ (blue starred) and (b) Modified compressed Multitone QAM symbols constellations with $\beta_c \leq 1$ (blue starred) with respect to conventional Multitone QAM symbols constellations (orange dots) for $M = 16$.

constellation symbols from (6) and $\boldsymbol{B}_{\sqrt{M}}$ can be represented as

$$\boldsymbol{B}_{\sqrt{M}} = \begin{bmatrix} b_1 & 0 & 0 & \cdots & 0 \\ 0 & b_2 & 0 & \cdots & 0 \\ 0 & 0 & b_3 & \cdots & 0 \\ \vdots & \vdots & \vdots & \ddots & \vdots \\ 0 & 0 & 0 & \cdots & b_{\sqrt{M}} \end{bmatrix}. \tag{14}$$

Let α and β be considered as parameters to convert the symmetric symbol constellation to an asymmetric constellation. α is considered to redesign the $M/4$ inner constellation points for QAM, i.e., $s_{2,2}$, $s_{2,3}$, $s_{3,2}$, and $s_{3,3}$ for $M = 16$ whereas β is considered to redesign the remaining $3M/4$ outer constellation points to result in an overall asymmetric QAM symbol constellation. Let $\boldsymbol{\alpha}_{\sqrt{M}}$ be a $\frac{\sqrt{M}}{2} \times 1$ column vector consisting of the parameter α as

$$\boldsymbol{\alpha}_{\sqrt{M}} = \begin{bmatrix} \alpha \\ \alpha \\ \vdots \\ \alpha \end{bmatrix} \tag{15}$$

and $\boldsymbol{\beta}_{\sqrt{M}}$ be a $\frac{\sqrt{M}}{4} \times 1$ column vector consisting of the parameter β as

$$\boldsymbol{\beta}_{\sqrt{M}} = \begin{bmatrix} \beta \\ \beta \\ \vdots \\ \beta \end{bmatrix}. \tag{16}$$

Then the $\sqrt{M} \times 1$ column vector $\boldsymbol{\Delta B}_{\sqrt{M}}$ can be used for designing asymmetric $\sqrt{M}$-PAM constellation and by (15) and (16), can be defined as

$$\boldsymbol{\Delta B}_{\sqrt{M}} = \begin{bmatrix} \boldsymbol{\beta}_{\sqrt{M}} \\ \boldsymbol{\alpha}_{\sqrt{M}} \\ \boldsymbol{\beta}_{\sqrt{M}} \end{bmatrix}. \tag{17}$$

From (14) and (17), the redesigned asymmetric $\sqrt{M}$-PAM constellation can be obtained as

$$\boldsymbol{B}_{\text{asym},\sqrt{M}} = \boldsymbol{B}_{\sqrt{M}} \times \boldsymbol{\Delta B}_{\sqrt{M}}. \tag{18}$$

Further, $\sqrt{M}$-PAM constellation in (18) can be used to design asymmetric QAM symbol constellation.

B. EXPANDED MULTITONE QAM SYMBOLS CONSTELLATIONS

α modifies the $M/4$ inner symbols and β modifies the $3M/4$ outer symbols. In the case of the increased symbol energy for outer symbols, β needs to be greater than 1. For this, α would be lower than 1 considering the same overall average symbol energy. The resulting modified symbol constellation would be expanded compared to the conventional QAM constellation. Here, all symbol phases are considered the same as the conventional constellation without redesign.

Let α_e and β_e be the modifying parameters for expanded constellation symbols i.e., the increased maximum available energy of the outer symbols. For $\alpha_e \leq 1$, β_e for a modified symbol constellation with the same average symbol energy can be represented as

$$\beta_e = \frac{4 + 2\sqrt{5} + \alpha_e}{3 + 2\sqrt{5}}. \tag{19}$$

Fig. 7(a) illustrates a modified expanded constellation where inner $M/4$ symbols are compressed and outer $3M/4$ outer symbols are expanded.

Multitone QAM symbol constellations with $M = 16$ for different cases of $\alpha_e = 0.9$, $\alpha_e = 0.7$, $\alpha_e = 0.5$, and $\alpha_e = 0.3$ using (17) and (18) are shown in Fig. 8. It can be seen

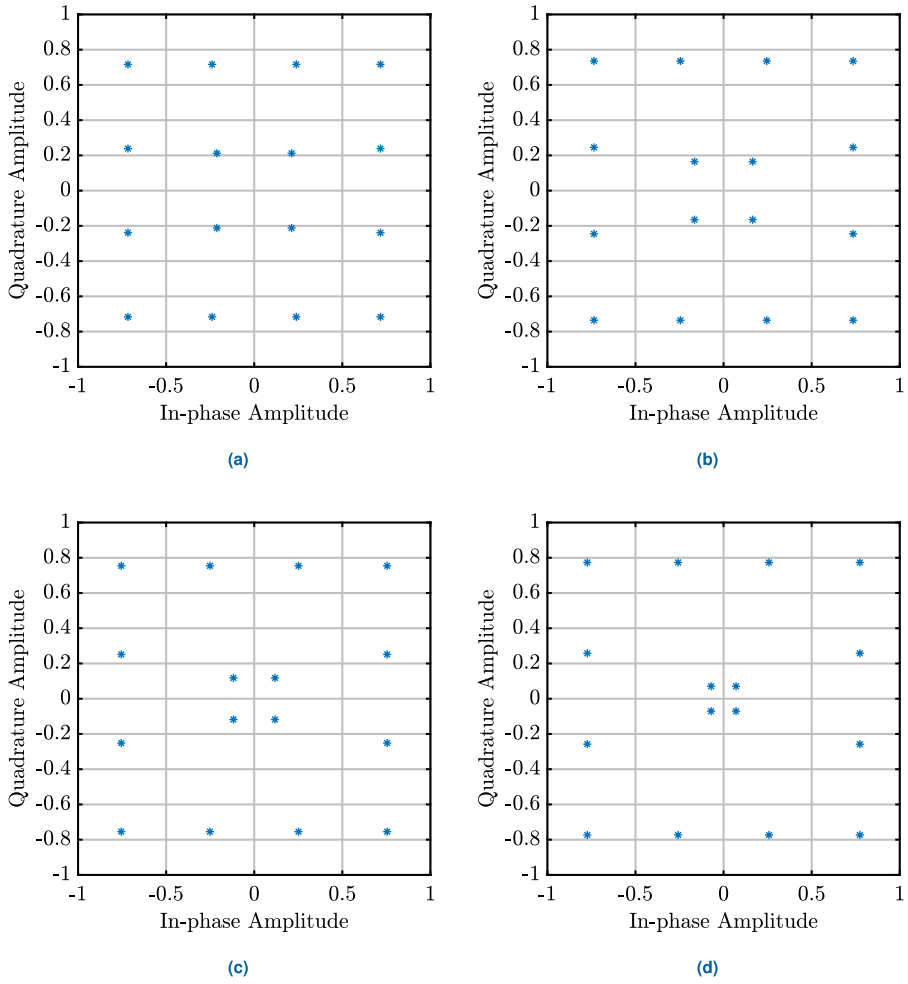

FIGURE 8. Multitone QAM expanded symbols constellations for (a) $\alpha_e = 0.9$, (b) $\alpha_e = 0.7$, (c) $\alpha_e = 0.5$, and (d) $\alpha_e = 0.3$, for $M = 16$.

that as the α_e is reduced β_e increases. The amount with which the inner symbols are compressed is higher than the amount with which outer symbols are expanded as $M/4$ symbols compression is balanced by the expansion of $3M/4$ symbols for the same average symbol constellation energy.

C. COMPRESSED MULTITONE QAM SYMBOLS CONSTELLATIONS

If the minimum available symbol energy is increased, the outer symbols' energy would be decreased for the same average symbol energy of the constellation, resulting in an overall compressed symbol constellation. Let β_c be the compression factor for outer $3M/4$ symbols, then α_c be the factor for inner $M/4$ symbols can be represented by

$$\alpha_c = (4 + 2\sqrt{5}) - (2 + \sqrt{5})\beta_c. \tag{20}$$

Fig. 7(b) illustrates a modified compressed constellation where inner $M/4$ symbols are expanded, i.e., minimum symbol magnitude increased and outer $3M/4$ symbols are compressed, i.e., maximum available symbol magnitude decreased. As the outer symbols are compressed, resulting in the expanded inner symbols for the same average symbol constellation energy, there must be a compression limit so that the inner symbols' magnitudes do not replace the outer symbols and the limit over β_c can be represented as

$$\frac{\alpha_c}{3} < \beta_c \leq 1. \tag{21}$$

Multitone QAM symbol constellations with $M = 16$ for different cases of $\beta_c = 0.88$, $\beta_c = 0.9$, $\beta_c = 0.92$, and $\beta_c = 0.96$ using (17) and (18) are shown in Fig. 9. It can be seen that as the β_c is reduced, α_c increases resulting in a higher minimum available symbol energy. As $3M/4$ outer symbols compression is balanced by the expansion of $M/4$ inner symbols for the same average symbol constellation energy, inner symbols energy increases with a larger amount compared to the decrease in the outer symbol energy and can be observed by Fig. 9(d) for $\beta_c = 0.88$.

IV. PERFORMANCE ANALYSIS OF MULTITONE QAM

Utilization of the same RF signal for information transfer, in addition to the power transfer, somewhat reduces the transferred power at the rectifier output. However, it offers an additional benefit of transferring the data as well as power simultaneously. Here, power conversion efficiency is

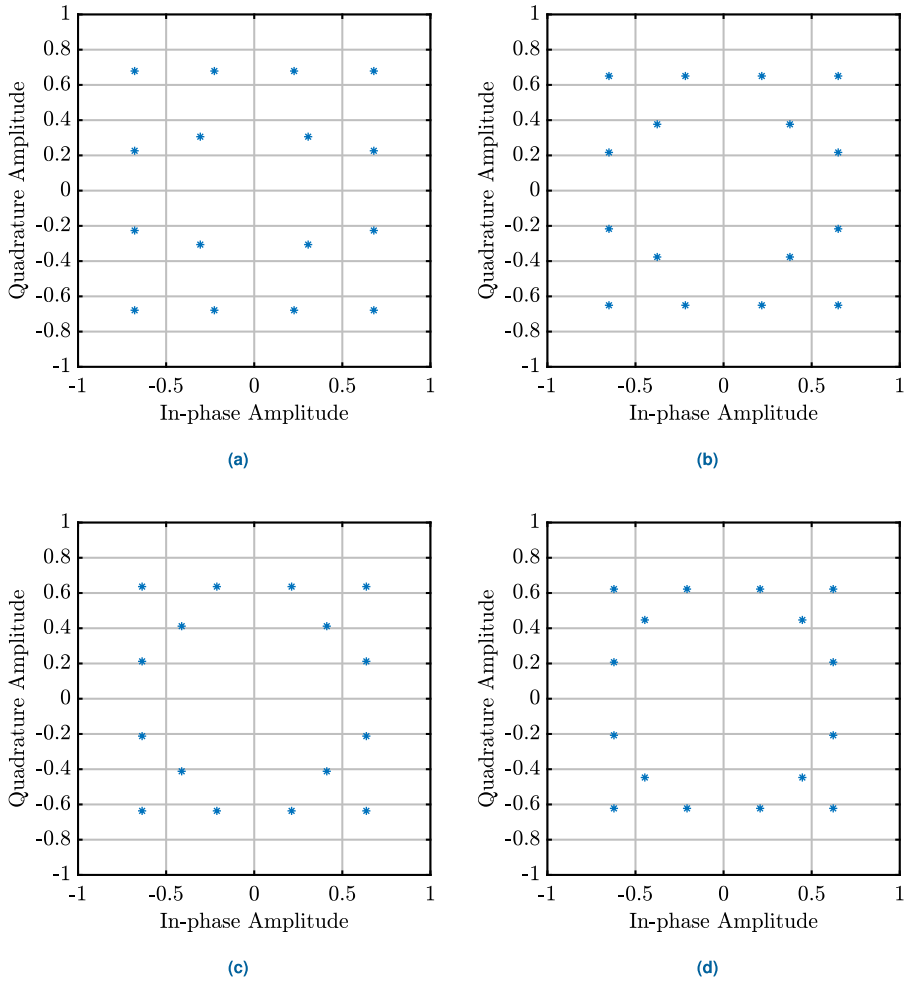

FIGURE 9. Multitone QAM compressed symbols constellations for (a) $\beta_c = 0.96$, (b) $\beta_c = 0.92$, (c) $\beta_c = 0.9$, and (d) $\beta_c = 0.88$, for $M = 16$.

considered a metric for measuring the WPT performance of the designed Multitone QAM signal. Performance of the designed Multitone QAM signal is evaluated over an information-energy rectifier receiver model depicted in Fig. 1. The rectifier model is implemented in Keysight ADS and was experimentally validated by measurements in the paper [27].

The rectifier-receiver model consists of the input matching network with stubs and an input capacitance of 0.1 pF, two Skyworks SMS7630-079LF Schottky diodes, and an RC-LPF with an output capacitance of 0.1 pF and output load of $R_{\text{load}} = 4.4$ kΩ. For SWIPT, the rectifier-receiver model needs to be designed from both wireless power transfer and wireless information transfer perspectives. The rectifier is required to have maximum PCE over a large bandwidth to make the transmission of multitone signal with a large number of tones feasible for an increased throughput for wireless information transfer performance of the SWIPT system. Here, the rectifier is designed to maximize PCE over a large matched bandwidth of around 100 MHz. This is achieved by optimizing PCE and reflection coefficient with the help of stub lengths, input capacitance, and output load R_{load}. Also, LPF is designed to filter out fundamental tones and all the harmonics while simultaneously having a sufficiently large bandwidth to pass the second-order baseband intermodulation frequency components IM_2s used for information decoding at the receiver. Load resistance is selected according to this, and it is considered to be a fixed value. WIT performance deteriorates if the LPF cutoff frequency is selected too narrow as now, relevant baseband tones carrying information would suffer attenuation.

Multitone QAM tone frequencies are selected as asymmetrically spaced tones as discussed in [27]. For example, tone frequencies for a 6-tone Multitone QAM signal centered around 2.45 GHz results in 2.440 GHz, 2.441 GHz, 2.443 GHz, 2.447 GHz, 2.452 GHz, and 2.460 GHz with a Greatest commom divisor, GCD = 1 MHz from Algorithm 1 of [27]. The PCE at the rectifier output from Fig. 1 in terms of rectified signal DC power y_{dc} of $y(t)$, output load R_{load} of RC-LPF, and resulting average power P_{avg} of transmitted signal can be represented by

$$\text{PCE} = \frac{|y_{\text{dc}}|^2/R_{\text{load}}}{P_{\text{avg}}} \times 100. \tag{22}$$

All multitone QAM results are obtained with the help of Keysight ADS rectifier receiver model and MATLAB. The multitone QAM signal is designed to have a bandwidth smaller than the RF matching bandwidth of the rectifier-receiver model. In this transmission scheme, $(N-1)$ information symbols are transmitted over a single N-tone multitone signal. Therefore, throughput can be represented as

$$\text{Throughput} = \frac{(N-1)\times \log_2 M}{T_{\text{QAM}}}, \tag{23}$$

where T_{QAM} is the time period of the Multitone QAM signal. Here, the effect of transmission distance on transmission efficiency has not been considered. The focus of the work has been the proposal of a Multitone QAM transmission scheme for SWIPT where both wireless power transfer and wireless information transfer are performed on the same rectified signal through the integrated information-energy rectifier receiver. To evaluate the over-the-air performance of the proposed scheme with distance, the effect of the channel would require to be considered. This can be investigated in future work for further performance evaluation. Accordingly, appropriate coding schemes can be utilized for performance enhancement.

Fig. 10 illustrates the output PCE variation with the average input power P_{in} for two cases: when the 6-tone multitone signal is solely used for power transfer and when the 16-QAM 6-tone multitone signal is used to carry the information data with a transmission rate of 20 Mbps in addition to power transfer simultaneously. The transmission rate of 20 Mbps is evaluated from (23) for $N = 6$, $M = 16$, and GCD $= 1$ MHz resulting in $T_{\text{QAM}} = 1\,\mu$sec. The performance is evaluated for 350 multitone streams, i.e., 1750 information symbols, i.e., 7000 bits. For low-input power levels, the signal's power conversion efficiency is quite low as the signal is not able to cross the diode's threshold voltage. Subsequently, PCE further increases with increasing input power levels and starts decreasing after a certain input power level (in our case $P_{\text{in}} = 0$ dBm). The output PCE performance is input power dependent, but the aim is to use the rectifier in the most optimal input power range to maximize PCE. Our modulated Multitone QAM waveform brings an additional degree of freedom to tailor PCE and BER. Multitone QAM allows the tuning of PCE and information rate as a function of the input power level to help overcome this fundamental limitation of WPT. For example, for low input powers, it is possible to select a waveform by varying different parameters that improve PCE more compared to the information transfer rate.

It can be seen that the maximum achievable PCE has been reduced for the Multitone QAM SWIPT signal compared to the obtained PCE for the RF signal for WPT transfer only. Therefore, the simultaneous flow of information over the multitone signal results in a slightly lower power efficiency, resulting in a trade-off between WPT performance and WIT performance for the overall SWIPT performance of the signal. The attainable output PCE is affected by the transmitted information symbols magnitudes variations of different tones of the multitone signal. For M-QAM information transfer, M information symbols have different magnitudes. Consequently, the average power of the transmitted Multitone QAM signal depends upon the transmitted information symbols. The WPT performance of the system would be higher when the outer $3M/4$ information symbols with higher magnitudes are transmitted compared to the cases where the inner $M/4$ information symbols are transmitted. Therefore, it is necessary to minimize the difference between the achievable PCE of the rectifier for different transferred symbols. For this, a redesigning of QAM symbol constellations for a more stable output PCE is required, as discussed in Section III.

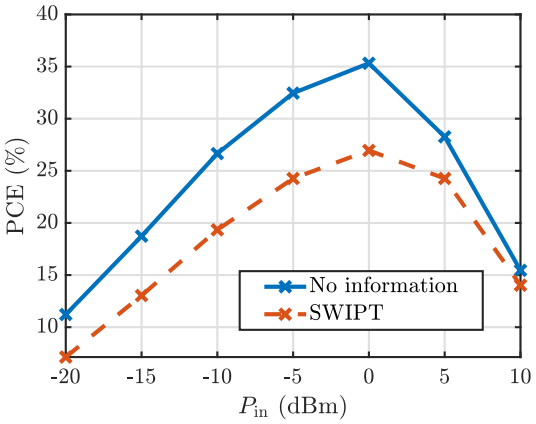

FIGURE 10. PCE for a 6-tone multitone signal without information data and with a 16-QAM simultaneous information flow with a transmission rate of 20 Mbps varying with average input power P_{in}.

Fig. 11 shows the achievable PCE for a 6-tone multitone signal at $P_{\text{in}} = 0$ dBm when the outer $3M/4$ information symbols are transmitted using asymmetric expanded 16-QAM symbol constellation with a transmission rate of 20 Mbps as discussed in Section III-B. It can be seen that a PCE of a maximum of 37.7% can be achieved when no information is being transmitted over the RF multitone signal. This maximum possible efficiency of the rectifier depends upon the designed rectifier circuitry and may further be increased with an improved structure. With the transmission of the outer $3M/4$ symbols of the conventional symmetric QAM symbols constellation, a maximum of 35.9% PCE can be achieved. This attainable power efficiency for the outer $3M/4$ higher magnitudes can be increased by the asymmetric expanded 16-QAM symbol constellation of Fig. 7(a). In Fig. 11, it can be seen that PCE performance for outer symbols increases with the reduction in α_{e}. The reason for this is the increased possible higher magnitudes for $3M/4$ symbols with the reduction in α_{e}. It can also be observed that with decreasing α_{e}, obtained PCE can be higher compared to the case of multitone signal $r(t)$ where no information is transmitted. This is due to the increased magnitude of outer symbols as α_{e} decreases.

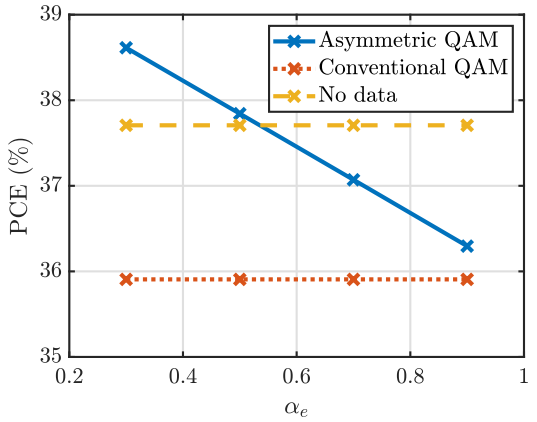

FIGURE 11. PCE comparison for a 6-tone multitone signal with no information flow, using conventional QAM, and the asymmetric expanded QAM symbols constellations for outer symbols with $M = 16$ with a transmission rate of 20 Mbps and average input power $P_{\text{in}} = 0$ dBm.

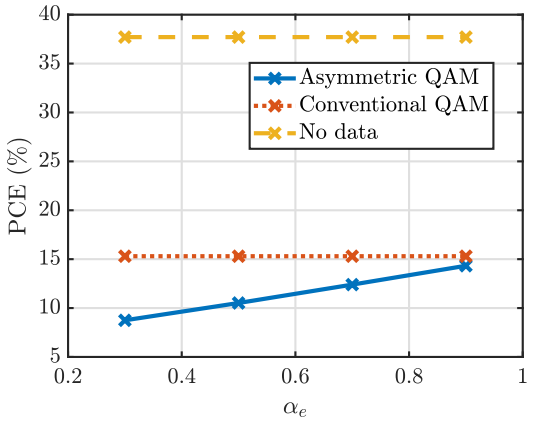

FIGURE 12. PCE comparison for a 6-tone multitone signal with no information flow, using conventional QAM, and the asymmetric expanded QAM symbols constellations for inner symbols with $M = 16$ with a transmission rate of 20 Mbps and average input power $P_{\text{in}} = 0$ dBm.

Similarly, Fig. 12 illustrates a comparison of achievable PCE for a 6-tone multitone signal at $P_{\text{in}} = 0$ dBm where the inner $M/4$ information symbols are transmitted using 16-QAM asymmetric symbol constellation with a transmission rate of 20 Mbps. It can be seen that WPT performance reduces from 37.7% to 15.31% when the inner information symbols of the conventional symmetric QAM symbol constellation of Fig. 5(a) are transmitted. The usage of asymmetric QAM constellation further reduces the WPT performance for the inner $M/4$ symbols as transmitted magnitudes reduce with the reduced α_{e} and are maximum when $\alpha_{\text{e}} = 1$, i.e., for conventional QAM. Therefore, SWIPT system performance can be improved with the help of expanded symbols constellations when the outer $3M/4$ symbols having larger magnitudes have a higher probability of transmission compared to the $M/4$ inner symbols. From the WIT perspective, as α_e reduces, the probability of detection error for the inner $M/4$ symbols decreases due to the lower distance between inner symbols as shown in Fig. 8(c). However, for the outer $3M/4$ symbols, the probability of error reduces with the reduction in α_e because of the increased distance between outer symbols. For the case of a very low α_e, increased detection error for inner symbols can be compensated with additional support vector machine (SVM) data classification and detection techniques [35].

Further, Fig. 13 compares the PCE performance of a 6-tone multitone QAM signal with a transmission rate of 20 Mbps using asymmetric compressed 16-QAM constellation (depicted in Fig. 7(b)) with conventional symmetric QAM constellation, and with no information flow at $P_{\text{in}} = 0$ dBm. It can be seen that PCE performance for outer $3M/4$ symbols reduces slightly with the reduction in compression parameter β_{c} and is maximum $\beta_{\text{c}} = 1$ for the conventional QAM constellation, i.e., from 36% for conventional 16-QAM to 32.4% for compressed 16-QAM for $\beta_{\text{c}} = 0.88$. However, PCE performance for inner $M/4$ symbols improves to around 24.5% for $\beta_{\text{c}} = 0.88$ compared to 15.31% for the conventional QAM as shown in Fig. 14. Therefore, for the case of the asymmetric compressed constellation, minimum power transfer using a multitone QAM signal can be increased with a small compromise in terms of maximal achievable PCE. β_c maybe selected close to the lowest possible values represented by (21) for the applications where minimum transferred power is of main concern. In such a case, WIT performance may get worse as symbols are now very close to each other, as shown in Fig. 9(d). Additional SVM-based classification and detection techniques can be utilized to improve the WIT performance [35].

From the WIT perspective, as α_e reduces, the probability of detection error for the inner $M/4$ symbols decreases due to the lower distance between inner symbols as shown in Fig. 8(c). However, for the outer $3M/4$ symbols, the probability of error reduces with the reduction in α_e because of the increased distance between outer symbols. For the case of a very low α_e, increased detection error for inner symbols can be compensated with additional detection techniques such as support vector machine (SVM) detection. Therefore, the impact of information transfer on PCE can be reduced by using the asymmetric symbol constellation at the cost of a higher symbol error rate.

Further, an optimum value of α_{e} or β_{c} can be selected depending on the probabilities of the transmission of the inner and outer symbols and depending upon the desired SWIPT performance. Till now, QAM constellations consist of symbols having equal probability. To observe the utilization of α_{e} and β_{c}, a non-uniform probability distribution among inner and outer symbols is considered. Let inner $M/4$ symbols have the probability of occurrence $\Pr(s_{\text{inner}})$. Then, the outer $3M/4$ symbols probability $\Pr(s_{\text{outer}})$ can be calculated as

$$\Pr(s_{\text{outer}}) = \frac{4 - M\Pr(s_{\text{inner}})}{3M}. \tag{24}$$

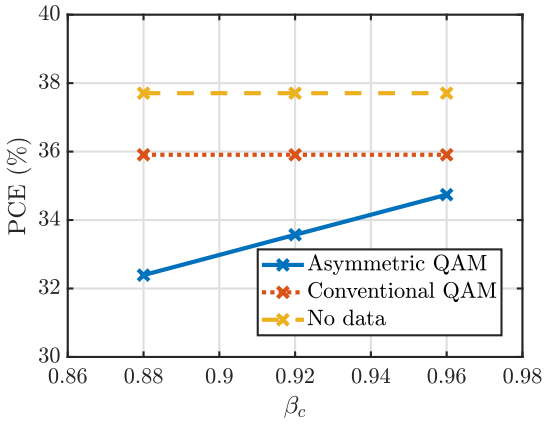

FIGURE 13. PCE comparison for a 6-tone multitone signal with no information flow, using conventional QAM, and the asymmetric compressed QAM symbols constellations for outer symbols with $M = 16$ with a transmission rate of 20 Mbps and average input power $P_{in} = 0$ dBm.

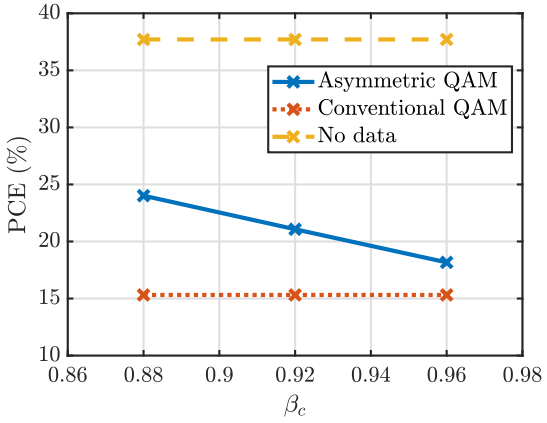

FIGURE 14. PCE comparison for a 6-tone multitone signal with no information flow, using conventional QAM, and the asymmetric compressed QAM symbols constellations for inner symbols with $M = 16$ with a transmission rate of 20 Mbps and average input power $P_{in} = 0$ dBm.

Fig. 15 illustrates the variation in the output PCE for 6-tone multitone QAM signal with the expanded QAM symbols as well as for the compressed QAM for unequal probabilities between inner and outer symbols. It can also be seen that the minimum level of power transfer can be increased by the usage of compressed QAM symbols. For example, $\beta_c = 0.92$ performs better than $\alpha_e = 0.7$ when inner symbols probability $\Pr(s_{inner}) = p$ is also significant. Further, it can be observed that the maximum possible power transfer can be increased by the use of the expanded symbol constellation, i.e., $\alpha_e = 0.7$ performs better than the case of $\beta_c = 0.92$ for the maximum possible power transfer.

Expanded asymmetric constellation provides enhanced WIT performance compared to compressed asymmetric constellations due to the increased distance between the symbols in the former case. Therefore, a compromise over system WPT performance is made with a multitone QAM

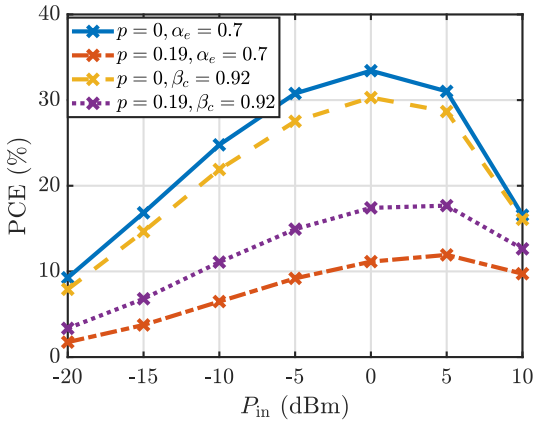

FIGURE 15. PCE comparison for a 6-tone multitone signal with 16-QAM expanded constellation ($\alpha_e = 0.7$) and compressed constellation ($\beta_c = 0.92$) for $\Pr(s_{inner}) = p$ for a transmission rate of 20 Mbps.

signal. However, it provides an additional benefit of information transmission using the same resources. An expanded or compressed information symbols constellation can be utilized according to a desired WPT and WIT performance.

For different application demands, different transmission scenarios under these asymmetric constellations can be selected. For example, it is possible to have an output PCE close to the maximum possible PCE of the rectifier for the outer $3M/4$ symbols with the help of an expanded symbol constellation which improves the information rate or number of bits per symbol (Fig. 11), i.e., it is possible to achieve maximum PCE while simultaneously transferring a data rate of 20 Mbps for a 6-tone multitone signal, but this is only possible with low symbol error rate at very high received signal powers. Asymmetric compressed QAM symbol constellation helps to increase the minimum transferred power level with the same data rate of 20 Mbps for a 6-tone multitone signal (Fig. 14) but would result in a higher symbol error rate. Therefore, the trade-off between the symbol error rate, modulation order (data rate), and power demands can be utilized according to the application's specific demands.

Furthermore, probabilities of symbol transmission (inner $M/4$ symbols and outer $3M/4$ symbols) can be varied to enhance the performance. Parameters can be selected based on the IoT device's operating conditions, such as whether consistent minimum power transfer is critical or if a high-power transfer in short bursts is preferred for the SWIPT's operation.

V. CONCLUSION

In this paper, a novel Multitone QAM transmission scheme utilizing multitone signal's amplitudes, phases, and number of tones for the integrated information-energy SWIPT architecture has been proposed. Both amplitudes and phases of tones of the multitone signal are utilized for the information encoding, resulting in a higher data rate. Multiple symbols are transmitted simultaneously over a single stream of

N-tone multitone QAM signal, resulting in an OFDM-type communication with non-uniform frequency spacings. The effect of orientation of the QAM symbol constellation has been analyzed over the PAPR of the designed waveform. Further, varying magnitudes of the QAM symbols constellation have been shown to affect WPT performance significantly. Two asymmetric QAM constellation designs, expanded symbol constellation and compressed symbol constellation, are proposed are proposed to allow trade-offs of application-specific demands such as power demands, symbol error rate, and data rate. Further, probabilities of transmission probabilities of inner symbols and outer symbols can be varied to enhance the performance.

For frequency selective channels and under multipath fading scenarios, phase distortion would occur, and different tones would undergo different attenuation. In the future, the effect of the channel over WPT and WIT performances needs to be studied more on the designed SWIPT waveforms and further optimize according to the channel conditions. Practically, WSNs consist of heterogeneous networks where each of the sensor nodes is operating for various applications and has different energy and information demands. Therefore, transmission waveforms need to be optimized according to the specific applications, and multimode receivers can be utilized in practical SWIPT systems.

REFERENCES

[1] I. Zhou, I. Makhdoom, N. Shariati, M. A. Raza, R. Keshavarz, J. Lipman, M. Abolhasan, and A. Jamalipour, "Internet of Things 2.0: Concepts, applications, and future directions," *IEEE Access*, vol. 9, pp. 70961–71012, 2021.

[2] A. Costanzo, D. Masotti, G. Paolini, and D. Schreurs, "Evolution of SWIPT for the IoT world: Near- and far-field solutions for simultaneous wireless information and power transfer," *IEEE Microw. Mag.*, vol. 22, no. 12, pp. 48–59, Dec. 2021.

[3] P. Dhull, A. P. Guevara, M. Ansari, S. Pollin, N. Shariati, and D. Schreurs, "Internet of Things networks: Enabling simultaneous wireless information and power transfer," *IEEE Microw. Mag.*, vol. 23, no. 3, pp. 39–54, Mar. 2022.

[4] T. D. P. Perera, D. N. K. Jayakody, S. K. Sharma, S. Chatzinotas, and J. Li, "Simultaneous wireless information and power transfer (SWIPT): Recent advances and future challenges," *IEEE Commun. Surveys Tuts.*, vol. 20, no. 1, pp. 264–302, 1st Quart., 2018.

[5] X. Zhou, R. Zhang, and C. K. Ho, "Wireless information and power transfer: Architecture design and rate-energy tradeoff," *IEEE Trans. Commun.*, vol. 61, no. 11, pp. 4754–4767, Nov. 2013.

[6] X. Zhou, R. Zhang, and C. K. Ho, "Wireless information and power transfer in multiuser OFDM systems," *IEEE Trans. Wireless Commun.*, vol. 13, no. 4, pp. 2282–2294, Apr. 2014.

[7] I. Krikidis, S. Timotheou, S. Nikolaou, G. Zheng, D. W. K. Ng, and R. Schober, "Simultaneous wireless information and power transfer in modern communication systems," *IEEE Commun. Mag.*, vol. 52, no. 11, pp. 104–110, Nov. 2014.

[8] P. Mukherjee, C. Psomas, and I. Krikidis, "Chaotic waveform-based signal design for noncoherent SWIPT receivers," *IEEE Trans. Wireless Commun.*, vol. 23, no. 9, pp. 11831–11846, Sep. 2024.

[9] J.-G. Kim, G. Wei, M.-H. Kim, H.-S. Ryo, P.-C. Ri, and C. Zhu, "A splitting frequencies-based wireless power and information simultaneous transfer method," *IEEE Trans. Circuits Syst. I, Reg. Papers*, vol. 65, no. 12, pp. 4434–4445, Dec. 2018.

[10] A. Rajaram, J. Guerreiro, R. Dinis, D. N. K. Jayakody, and M. Beko, "Optimum performance analysis and receiver design for OFDM based frequency-splitting SWIPT with strong nonlinear effects," *IEEE Internet Things J.*, vol. 10, no. 23, pp. 20928–20940, Jun. 2023.

[11] C. R. Valenta and G. D. Durgin, "Harvesting wireless power: Survey of energy-harvester conversion efficiency in far-field, wireless power transfer systems," *IEEE Microw. Mag.*, vol. 15, no. 4, pp. 108–120, Jun. 2014.

[12] N. Shariati, J. R. Scott, D. Schreurs, and K. Ghorbani, "Multitone excitation analysis in RF energy Harvesters—Considerations and limitations," *IEEE Internet Things J.*, vol. 5, no. 4, pp. 2804–2816, Aug. 2018.

[13] A. Collado and A. Georgiadis, "Optimal waveforms for efficient wireless power transmission," *IEEE Microw. Wireless Compon. Lett.*, vol. 24, no. 5, pp. 354–356, May 2014.

[14] B. Clerckx, R. Zhang, R. Schober, D. W. K. Ng, D. I. Kim, and H. V. Poor, "Fundamentals of wireless information and power transfer: From RF energy harvester models to signal and system designs," *IEEE J. Sel. Areas Commun.*, vol. 37, no. 1, pp. 4–33, Jan. 2019.

[15] J. Kim and B. Clerckx, "Wireless information and power transfer for IoT: Pulse position modulation, integrated receiver, and experimental validation," *IEEE Internet Things J.*, vol. 9, no. 14, pp. 12378–12394, Jul. 2022.

[16] J. Kim, B. Clerckx, and P. D. Mitcheson, "Signal and system design for wireless power transfer: Prototype, experiment and validation," *IEEE Trans. Wireless Commun.*, vol. 19, no. 11, pp. 7453–7469, Nov. 2020.

[17] B. Clerckx and E. Bayguzina, "Waveform design for wireless power transfer," *IEEE Trans. Signal Process.*, vol. 64, no. 23, pp. 6313–6328, Dec. 2016.

[18] D. I. Kim, J. H. Moon, and J. J. Park, "New SWIPT using PAPR: How it works," *IEEE Wireless Commun. Lett.*, vol. 5, no. 6, pp. 672–675, Dec. 2016.

[19] I. Krikidis and C. Psomas, "Tone-index multisine modulation for SWIPT," *IEEE Signal Process. Lett.*, vol. 26, no. 8, pp. 1252–1256, Aug. 2019.

[20] C. Im, J.-W. Lee, and C. Lee, "A multi-tone amplitude modulation scheme for wireless information and power transfer," *IEEE Trans. Veh. Technol.*, vol. 69, no. 1, pp. 1147–1151, Jan. 2020.

[21] S. Claessens, N. Pan, M. Rajabi, D. Schreurs, and S. Pollin, "Enhanced biased ASK modulation performance for SWIPT with AWGN channel and dual-purpose hardware," *IEEE Trans. Microw. Theory Techn.*, vol. 66, no. 7, pp. 3478–3486, Jul. 2018.

[22] D.-Y. Kim, H.-S. Lee, K.-W. Kim, and J.-W. Lee, "Dual amplitude shift keying with double half-wave rectifier for SWIPT," *IEEE Wireless Commun. Lett.*, vol. 8, no. 4, pp. 1020–1023, Aug. 2019.

[23] A. Hanif and M. Doroslovač ki, "Simultaneous terahertz imaging with information and power transfer (STIIPT)," *IEEE J. Sel. Topics Signal Process.*, vol. 17, no. 4, pp. 806–818, Jul. 2023.

[24] M. Rajabi, N. Pan, S. Claessens, S. Pollin, and D. Schreurs, "Modulation techniques for simultaneous wireless information and power transfer with an integrated rectifier–receiver," *IEEE Trans. Microw. Theory Techn.*, vol. 66, no. 5, pp. 2373–2385, May 2018.

[25] S. Claessens, N. Pan, D. Schreurs, and S. Pollin, "Multitone FSK modulation for SWIPT," *IEEE Trans. Microw. Theory Techn.*, vol. 67, no. 5, pp. 1665–1674, May 2019.

[26] T. Ikeuchi and Y. Kawahara, "Peak to average power ratio based signal detection for frequency shift multitone SWIPT system," *IEEE Access*, vol. 9, pp. 4158–4172, 2021.

[27] P. Dhull, D. Schreurs, G. Paolini, A. Costanzo, M. Abolhasan, and N. Shariati, "Multitone PSK modulation design for simultaneous wireless information and power transfer," *IEEE Trans. Microw. Theory Techn.*, vol. 72, no. 1, pp. 446–460, Jan. 2024.

[28] K. Matsuura, K. Shin, D. Kobuchi, Y. Narusue, and H. Morikawa, "Synchronization strategy for distributed wireless power transfer with periodic frequency and phase synchronization," *IEEE Commun. Lett.*, vol. 27, no. 1, pp. 391–395, Jan. 2023.

[29] M. Rashid and J. A. Nanzer, "Frequency and phase synchronization in distributed antenna arrays based on consensus averaging and Kalman filtering," *IEEE Trans. Wireless Commun.*, vol. 22, no. 4, pp. 2789–2803, Apr. 2023.

[30] W. Jiang and Y. Cui, "Performance analysis of MPSK phase detectors for carrier synchronization PLLs at low SNRs," *IEEE Commun. Lett.*, vol. 18, no. 12, pp. 2133–2136, Dec. 2014.

[31] S. A. Maas, *Nonlinear Microwave Circuits Second Edition*. Norwood, MA, USA: Artech House, 2003.

[32] J. C. Pedro and N. B. Carvalho, *Intermodulation Distortion in Microwave and Wireless Circuits*. Norwood, MA, USA: Artech House, 2003.

[33] L. W. Couch, *Digital and Analog Communication Systems*, 8th ed., Upper Saddle River, NJ, USA: Pearson, 2012.
[34] A. S. Boaventura and N. B. Carvalho, "Maximizing DC power in energy harvesting circuits using multisine excitation," in *IEEE MTT-S Int. Microw. Symp. Dig.*, Jun. 2011, pp. 1–4.
[35] L. V. Nguyen, A. L. Swindlehurst, and D. H. N. Nguyen, "SVM-based channel estimation and data detection for one-bit massive MIMO systems," *IEEE Trans. Signal Process.*, vol. 69, pp. 2086–2099, 2021.

PRERNA DHULL (Graduate Student Member, IEEE) received the M.Tech. degree in electronics and communication engineering from Indian Institute of Technology Roorkee, Roorkee, India, in 2017. She is currently pursuing the double Ph.D. degree in electronics, RF, and communication technologies with KU Leuven, Leuven, Belgium, and the University of Technology Sydney, Sydney, NSW, Australia.

Her research interests include simultaneous wireless information and power transfer (SWIPT) systems, waveform design, wireless power transfer (WPT), energy harvesting, and self-sustainable networks. She was a recipient of the University of Technology Sydney Presidential Scholarship, the International Research Scholarship, the GRS Publication Fund, and the Thesis Completion Support Grant for her Ph.D. studies.

NEGIN SHARIATI (Senior Member, IEEE) received the Ph.D. degree in electrical-electronics and communication technologies from the Royal Melbourne Institute of Technology (RMIT), Australia, in 2016.

Prior to that, she worked in the industry as an Electrical-Electronics Engineer, from 2009 to 2012. She is currently an Associate Professor with the School of Electrical and Data Engineering, Faculty of Engineering and IT, University of Technology Sydney (UTS), Australia. She established the State-of-the-Art RF and Communication Technologies (RFCT) Research Laboratory, UTS, in 2018, where she is the Founding Director, leading research and development in RF technologies, sustainable sensing, energy harvesting, low-power Internet of Things (IoT), and AgTech. She led a three-year research and development program, "Sensing Innovations Constellation," at the Food Agility Cooperative Research Centre (CRC), which focused on three key interrelated streams: sensing, energy, and connectivity. This collaborative platform enabled multidisciplinary research and development with industry partners, addressing large-scale, and real-world challenges in agricultural technologies. She also served as the Director of the Women in Engineering and IT (WiEIT), Faculty of Engineering and IT, from 2023 to 2024, driving positive changes in equity and diversity in science, technology, engineering, and mathematics (STEM). Since 2018, she has held a joint academic appointment at Hokkaido University, Japan, engaging in research and teaching activities. Over the past three years, she has secured more than six million dollars in research funding across multiple Australian Research Council (ARC), CRC, industry, and government-funded research projects, where she has taken the lead Chief Investigator (CI) role and contributed as a CI Team Member. She leads a three-year multidisciplinary research and development program titled "Sustainable Sensing, Enhanced Connectivity, and Data Analytics for Precision Urban and Rural Agriculture" in collaboration with Nippon Telegraph and Telephone Corporation (NTT) and Food Agility CRC. Her research interests include RF/microwave/electronics circuits and systems, sensors, antennas, RF energy harvesting, simultaneous wireless information and power transfer, and wireless sensor networks.

SOFIE POLLIN (Senior Member, IEEE) is currently a Professor with KU Leuven, focusing on wireless communication systems. Before that, she worked with IMEC and the University of California at Berkeley. She is also a Principal Member of the Technical Staff with IMEC. Her research centers around wireless networks that require networks that are ever more dense, heterogeneous, battery-powered, and spectrum-constrained. Her research interests include cell-free networks, integrated communication and sensing, and non-terrestrial networks.

MEHRAN ABOLHASAN (Senior Member, IEEE) received the B.E. degree in computer engineering and the Ph.D. degree in telecommunications from the University of Wollongong, in 1999 and 2003, respectively. He has over 20 years of experience in research and development and serving in various research leadership roles. Some of these previous roles include serving as the Director of research programs with the Faculty of Engineering and IT and the Deputy Head of the School for Research with the School of Electrical and Data Engineering, University of Technology Sydney. He is currently the Leader of the Intelligent Networks and Applications Laboratory, Faculty of Engineering and IT, University of Technology Sydney. He has authored over 180 international publications and through his sustained track record of industry engagement and the creation of new research ideas and directions. He has successfully secured several research and development projects worth over eight million dollars. This includes external grants, such as ARC, CRC, industry, and government-funded research projects. His current research interests include 5G/6G wireless networks, the Internet of Things, cybersecurity, software-defined networking, intelligent transportation systems (ITS), urban greening, and digital agriculture.

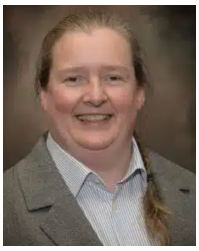

DOMINIQUE SCHREURS (Fellow, IEEE) received the M.Sc. and Ph.D. degrees in electronic engineering from KU Leuven, Leuven, Belgium, in 1992 and 1997, respectively.

She was a Postdoctoral Fellow and a Visiting Scientist with Agilent Technologies, Santa Clara, CA, USA; ETH Zürich, Zürich, Switzerland; and the National Institute of Standards and Technology (NIST), Boulder, CO, USA. She is currently a Full Professor with KU Leuven. Her research interests include microwave/mmWave metrology, device and circuit modeling, and subsystem design for wireless and biomedical applications.

Prof. Schreurs was the President of the Microwave Theory and Technology Society (MTT-S), from 2018 to 2019. She has been on IEEE MTT-S AdCom, since 2009, in multiple roles. She initiated the IEEE Women in Microwaves (WiM) Event at the European Microwave Week, in 2008, and has been acting as an Advisor for WiM Events ever since. She was the Technical Program Committee (TPC) Co-Chair for the International Microwave Symposium (IMS), in 2023, and the Conference Chair for the International Microwave Biomedical Conference (IMBioC), in 2023. She is the Past President of the ARFTG Organization and was involved in multiple ARFTG conferences as the conference chair and the TPC chair. She was a Distinguished Microwave Lecturer, from 2012 to 2014. She was the Editor-in-Chief of IEEE TRANSACTIONS ON MICROWAVE THEORY AND TECHNIQUES, from 2014 to 2016.